First Clinical Experience With [^{89}Zr]Zr-Df-IAB22M2C PET/MRI in Patients With Metastatic Cancer

Johannes Schwenck
Universitatsklinikum Tubingen Department fur Radiologie
Dominik Sonanini
University of Tübingen: Eberhard Karls Universitat Tubingen
Dominik Seyfried
Universitatsklinikum Tubingen Department fur Radiologie
Walter Ehrlichmann
Universitatsklinikum Tubingen Department fur Radiologie
Gabriele Kienzle
Universitatsklinikum Tubingen Department fur Radiologie
Gerald Reischl
Universitatsklinikum Tubingen Department fur Radiologie
Pascal Krezer
Universitatsklinikum Tubingen Department fur Radiologie
Ian Wilson
ImaginAb
Ron Korn
ImaginAb
Irene Gonzalez-Menendez
Universitatsklinikum Tubingen
Leticia Quintanilla-Martinez
Universitatsklinikum Tubingen
Ferdinand Seith
University Tübingen Department of Radiology: Universitatsklinikum Tubingen Department fur Radiologie
Andrea Forschner
Universitatsklinikum Tubingen
Thomas Eigentler
Universitatsklinikum Tubingen
Lars Zender
Universitätsklinikum Tübingen: Universitatsklinikum Tubingen
Martin Röcken
Universitatsklinikum Tubingen
Bernd Pichler
Universitatsklinikum Tubingen Department fur Radiologie
Lukas Flatz
Universitatsklinikum Tubingen
Manfred Kneilling
Universitatsklinikum Tubingen Department fur Radiologie
Christian la Fougère (christian.lafougere@med.uni-tuebingen.de)
Universitatsklinikum Tubingen Department fur Radiologie https://orcid.org/0000-0001-7519-0417

Research Article

Keywords:

Posted Date: February 24th, 2022

DOI: https://doi.org/10.21203/rs.3.rs-1369201/v1

Abstract

Aim/Introduction: Despite the spectacular success of immune checkpoint inhibitor therapy (ICT) in patients with metastatic cancer, only a limited proportion of patients benefit from ICT. An important gatekeeper for the therapeutic response to ICT are $CD8^+$ cytotoxic T cells which are able to recognize MHC class I-dependent tumor antigens and destroy tumor cells. The radiolabeled minibody [^{89}Zr]Zr-Df-IAB22M2C has a high affinity for human $CD8^+$ T cells and was already successfully tested in a phase I study. Here, we aimed to gain first clinical PET/MRI experience with the non-invasive assessment of the $CD8^+$ T cell distribution in cancer patients by *in vivo* [^{89}Zr]Zr-Df-IAB22M2C.

Material and Methods: We investigated 8 patients with metastasized cancers undergoing ICT. Radiolabeling of Df-IAB22M2C with Zr-89 was performed according to Good Manufacturing Practice. Multiparametric PET/MRI was acquired 24 h after injection of 74.2±17.9 MBq [^{89}Zr]Zr-Df-IAB22M2C. We analyzed the [^{89}Zr]Zr-Df-IAB22M2C uptake within the metastases and primary and secondary lymphatic organs.

Results: [^{89}Zr]Zr-Df-IAB22M2C injection was tolerated well without noticeable side effects. The CD8 PET/MRI data acquisitions 24 hours post administration of [^{89}Zr]Zr-Df-IAB22M2C revealed a good image quality with a relatively low background signal due to only low unspecific tissue uptake and marginal blood pool retention. Only two metastatic lesions showed a markedly increased tracer uptake in our cohort of patients. Furthermore, we observed a high interpatient variability in the [^{89}Zr]Zr-Df-IAB22M2C uptake within the primary and secondary lymphoid organs. Four out of five ICT patients exhibited a rather high [^{89}Zr]Zr-Df-IAB22M2C uptake in the bone marrow. Two of these four patients as well as two other patients yielded a pronounced [^{89}Zr]Zr-Df-IAB22M2C uptake within non metastatic lymph nodes. Interestingly, cancer progression in ICT patients was associated with a relatively low [^{89}Zr]Zr-Df-IAB22M2C uptake in the spleen compared to the liver in 4 out of the 6 patients.

Conclusion: Our first clinical experiences revealed the feasibility of [^{89}Zr]Zr-Df-IAB22M2C PET/MRI to assess potential immune-related changes in the metastases and the primary and secondary lymphatic organs. According to our results, we hypothesize that alteration in the [^{89}Zr]Zr-Df-IAB22M2C uptake in primary and secondary lymphoid organs might be associated with the response to ICT.

Introduction

The introduction of the immune checkpoint inhibitor therapy (ICT) in 2011 for metastatic melanoma represented a milestone in the treatment of advanced cancer. Previously, the prognosis of those patients was poor, with a 5-year survival rate of about 5% and an overall survival (OS) of about seven to eight months [1]. The use of monoclonal antibodies directed against the immune checkpoints CTLA4 (cytotoxic T-lymphocyte antigen 4, ipilimumab) and anti-PD-1 (programmed cell death protein 1, nivolumab and pembrolizumab) significantly improved both recurrence-free and OS of oncological patients. In individual cases, patients with relapse-free long-term survival have even been reported [1]. PD-1 and CTLA4 are inhibitory receptors expressed particularly on T cells. The antibody-mediated blockade of these inhibitory receptors reinvigorates the T cell response resulting in improved tumor control [2]. ICT is now a mainstay of systemic cancer therapy and firmly established in the relevant guidelines [3].

However, despite decreasing mortality rates in cancer patients treated with ICT, actually only a limited number of patients benefit from this expensive treatment approach. Only about 40% of melanoma patients respond to anti-PD-1 antibody monotherapy, while combining anti-CTLA4 and anti-PD-1 antibodies increases the response rate up to 60% [4, 5]. Regardless of treatment success, patients develop frequently immune-related adverse events (irAEs) that can lead to significant comorbidities in almost every organ including treatment related death [6, 7]. To date, no reliable predictive biomarker for ICT is available.

Activated effector $CD8^+$ T cells are an important prerequisite for successful ICT [8]. The spatial distribution of the $CD8^+$ cytotoxic T cells seems to play an important role both microscopically in the tumor [9] as well as macroscopically in the entire organism [10, 11]. A preexisting infiltration of $CD8^+$ T cells was shown to be crucial for an effective ICT [12] and therefore tumor-infiltrating $CD8^+$ T cells are considered to be a potential surrogate marker for response to ICT[13].

CD8 is a cell surface protein that functions as a co-receptor in antigen recognition on major histocompatibility complex class I (MHC I) molecules and is expressed on cytotoxic T cells, but also on some natural killer (NK) cells, natural killer T cells (NKT) and on certain populations of dendritic cells [14, 15]. $CD8^+$ T cells are found in most adult lymphoid tissues as well as in the blood where they perform their physiological task, e.g., in the defense against viral infections [16, 17].

The zirconium-89-desferrioxamine (^{89}Zr-DFO) labelled CD8-directed scFv-CH3 antibody fragment (minibody) [^{89}Zr]Zr-Df-IAB22M2C is characterized by a high affinity for human $CD8^+$ T cells enabling *in vivo* T cell tracking. In the dose escalation phase of the first phase I study six cancer patients were investigated with different [^{89}Zr]Zr-Df-IAB22M2C doses (0.2 mg-10 mg; 111 MBq) [18]. A dose-dependent tracer kinetic with high accumulations in lymphoid tissues such as spleen, bone marrow, and lymph nodes was observed by PET imaging between 2 and 148 h post injection (*p.i.*). Of note, increased tracer uptake in metastases was found only in two out of six patients [18]. In a recent publication including the dose expansion phase of the phase I trial with 9 additional patients an association between tumor uptake and response to immunotherapy was described in two melanoma patients under anti PD-1 therapy [19].

Here, we report on the first clinical experience with the non-invasive assessment of the $CD8^+$ T cell distribution, accumulation and homing patterns in metastatic cancer patients most of them upon ICT by simultaneous [^{89}Zr]Zr-Df-IAB22M2C PET/MRI. We aimed to assess patient specific differences in

$CD8^+$ T cell expression pattern within metastasis and the primary and secondary lymphatic organs to identify potential ICT-specific signatures.

Material And Methods

Following the stipulations of the German medicinal products act (*"Arzneimittelgesetz"*; AMG) § 13(2b) PET/MRI scans with [^{89}Zr]Zr-Df-IAB22M2C were performed in 8 patients with metastasized cancers (5 x cutaneous melanoma; 1 x choroidal melanoma, 1 x NSCLC and 1 x sarcoma). PET/MRI was preferred to PET/CT to reduce the radiation exposure. Three patients were eligible for ICT and the referring physicians requested the [^{89}Zr]Zr-Df-IAB22M2C PET imaging to aid the clinical decision towards ICT or therapeutic alternatives. Five patients were under ICT and clinical decisions towards prolongation, escalation or change of treatment needed to be addressed by the referring physicians. Six out of eight patients presented with progressive disease in the follow up after the [^{89}Zr]Zr-Df-IAB22M2C PET/MRI and were considered as non-responders. Patients 3 and 4 showed long term remission without detectable metastasis in the routine follow up for more than one year after the [^{89}Zr]Zr-Df-IAB22M2C PET/MRI (responders).

Radiolabeling

[^{18}F]FDG was manufactured in-house under a marketing license.

Patient individual preparations of [^{89}Zr]Zr-Df-IAB22M2C were performed following a modified procedure of Pandit-Taskar et al. [18] in a GMP environment. The precursor Df-IAB22M2C (80 kDa) was provided by ImaginAb Inc. (Inglewood, CA, USA), Zr-89 was manufactured by BV Cyclotron VU (Amsterdam, The Netherlands) and purchased from PerkinElmer (Rodgau, Germany). All other reagents, in highest quality available, were from common suppliers. Briefly, in a sterile, pyrogen free tube the acidic solution of [^{89}Zr]zirconium-oxalate was neutralized with 2 M sodium carbonate solution and buffered with 0.5 M ammonium acetate solution to a pH value of 6.5–7.5, then the Df-IAB22M2C precursor solution (protein concentration 2.7 mg/mL) was added. Amounts of ^{89}Zr activity and precursor were calculated from first test experiences (considering losses during preparation) to obtain the values described in material and methods chapter "*CD8 PET/MRI*" for a patient dose. After reaction for 40 min at ambient temperature 10 µL of DTPA solution (20%) was added to react with residual Zr-89 for 10 min. Efficiency of labeling was checked by TLC chromatography and autoradiography (≥ 94%, n = 8). Purification was done using size-exclusion-chromatography (disposable PD10 column, product code: 17085101, GE Healthcare). After elution of the product with the final formulation matrix (water for injection, 20 mM histidine, 5% (v/v) sucrose, 50 mM NaCl, 0.2 M L-arginine, pH 6.5), the product was sterile filtered and samples were taken for quality control. Every product batch was tested for the following parameters using validated methods (specifications in brackets): Appearance (clear, colorless, free of visible particles), pH (4.0–8.0), radiochemical purity tlc (≥ 90%), radiochemical purity size-exclusion HPLC (≥ 80%), radionuclidic purity, gamma spectrometry (≥ 99.9%), endotoxins (< 17.5 EU/mL, volume of patient dose ≤ 10 mL), immunoreactivity, bead assay (≥ 70%), sterility test (no growth). Every prepared batch met the specifications (n = 8).

CD8 PET/MRI

Multiparametric CD8 PET/MRI was performed 24 h after injection of 74.2 ± 17.9 MBq [89Zr]Zr-Df-IAB22M2C (1.1–1.8 mg Df-IAB22M2C) on a fully integrated 3T PET/MR system (Biograph mMR Siemens Healthineers, Erlangen, Germany). The previously published studies by Pandit-Taskar et al. and Farwell et al. reported a maximum tracer uptake 24-48h p.i. [18, 20] and in the context of patient convenience, we opted for PET/MRI data acquisition at 24 h p.i. iIn order to minimize radiation exposure to patients, we reduced the amount of tracer activity administered compared with available data in the literature to the previously reported (111 MBq [18, 20]).

PET data (4 min per bed position, four bed positions, cranial vertex to the thighs) were reconstructed using the vendor's software with 3D-OSEM algorithm, 21 subsets, 2 iterations, 256×256 matrix size (voxel size: 2.8×2.8×2.0 mm^3) and 4 mm Gaussian filter. A 3D T1-weighted spoiled gradient-echo sequence with Dixon-based fat-water separation in end-expiratory breath-hold was acquired to create an attenuation map. All attenuation maps were checked carefully for erroneous tissue identification. A fat saturated postcontrast T1 volumetric interpolated breath-hold examination (VIBE) was acquired in axial view with multiple breath-holds for anatomic correlation. Further sequences were acquired depending on clinical questions but were not part of the study evaluations.

Image analysis

CD8 PET/MRI data were reviewed by two board certified nuclear medicine specialists and discussed in consensus with the referring clinicians. For semi-quantitative analysis representative regions of interests (ROI) with 50% isocontour were defined by using a dedicated software package (Syngo.via, Siemens Healthineers, Erlangen and Affinity Viewer, Hermes Medical Solutions, Stockholm, Sweden). Lymphnodes and lesions with discernable tracer uptake compared to the background on fused PET/MR images were rated as positive for CD8 expression. Lesions were defined as malignant in concordance with the clinical reports of the available previous and subsequent routine imaging studies including [^{18}F]FDG PET/CT and CT scans.

Histology and immunohistochemistry

The morphological and immunohistochemical features were analyzed on formalin-fixed and paraffin-embedded tissue sections. Samples of Patient 1 and Patient 3 were stained with haematoxylin and eosin (H&E). Additionally, CD8 immunohistochemistry was performed on an automated immunostainer (Ventana Medical Systems, Tucson, AZ) according to the manufacturer's protocol using a CD8 antibody (clone C8/144B; Dako, Glostrup, Denmark). Appropriate positive and negative controls were used to confirm the adequacy of the staining. All samples were scanned with the Ventana

DP200 (Roche, Basel, Switzerland) and processed with the Image Viewer MFC Application. Final image preparation was performed with Adobe Photoshop CS6.

Results

The injection of 74.2 ± 17.9 MBq [^{89}Zr]Zr-Df-IAB22M2C was well tolerated in all patients without significant clinical side effects. In particular, we observe no allergic reactions, cutaneous erythema at the injection site, nausea, vomiting or circulatory problems from tracer injection until the end of the PET/MRI measurement. The PET/MRI acquisitions 24h *p.i.* revealed a good image quality. We noted marginal background signal due to a minor retention in the blood pool and some marginal unspecific tissue uptake.

In total, eight patients with metastatic cancer (cutaneous melanoma, n = 5; choroidal melanoma, n = 1; NSCLC, n = 1; sarcoma, n = 1) were assessed by means of PET/MRI before (n = 3) or under (n = 5) ICT (melanoma, n = 4; sarcoma, n = 1). Patients underwent anti CTLA-4 (ipilimumab, n = 1), anti PD-1 (nivolumab or pembrolizumab, n = 3) or combined checkpoint inhibition with ipilimumab and nivolumab (n = 1) (Table 1). Detailed findings of [^{89}Zr]Zr-Df-IAB22M2C PET/MRI are shown in Table 1. Only two melanoma patients (Patient 1 and Patient 7) exhibited an increased [^{89}Zr]Zr-Df-IAB22M2C uptake in metastasis compared to the background; all other metastases did not reveal any relevant tracer uptake.

Table 1

Patient	1	2	3	4	5	6	7	8
Cancer type	Cutaneous melanoma	Uveal melanoma	Cutaneous melanoma	Cutaneous melanoma	Bronchial cancer	Cutaneous melanoma	Cutaneous melanoma	Sarcoma
Therapy before scan	Ipilimumab	Surgery	Nivolumab	Surgery	None	Pembrolizumab	Ipilimumab/ Nivolumab	Nivolumab
Therapy after scan	Resection/ Nivolumab	Ipilimumab/ Nivolumab	Resection/ Nivolumab	Nivolumab	RCTx/Durvalumab	None	Nivolumab	Nivolumab
Outcome	Progress	Progress	Remission	Remission	Progress	Progress	Progress	Progress
Liver (SUVmean)	8.3	7.4	5.7	6.5	6.5	7.1	7.9	5.4
Spleen (SUVmean)	86.7	54.7	49.3	80.0	34.4	42.9	58.2	55.3
LN (SUVmean)	2.9	2.5	13.5	18.8	3.7	19.3	11.6	7.0
LN with highest uptake	retroperitoneal	cervical left	cervical left	liver hilum	axillar left	cervical left	cervical left	submandibular left
Lumbar vertebra (SUVmean)	10.6	4.7	10.1	6.9	5.5	7.4	10.8	12.3
Bloodpool (SUVmean)	1.6	1.4	1.7	1.5	1.7	1.5	1.2	1.5

RCTx (Radiochemotherapy); LN (Lymph node)

In Patient 1, CD8 PET/MRI was performed after three cycles of ipilimumab treatment, which was discontinued 6 weeks prior to the PET/MR scan due to recurrence of rheumatoid arthritis. CD8 PET/MRI revealed an intense [^{89}Zr]Zr-Df-IAB22M2C uptake in a progressive subcutaneous gluteal metastasis (Fig. 1A/B). Notably, a second progressive pararenal metastasis exhibited no relevant [^{89}Zr]Zr-Df-IAB22M2C uptake (Fig. 1C/D). Two other soft tissue lesions at the right thigh and presternal have been stable since at least 3 months and did not show any relevant [^{89}Zr]Zr-Df-IAB22M2C uptake.

Histopathological evaluation of the pararenal metastasis after surgical resection revealed a monotonous cell proliferation of the melanoma metastasis (Fig. 1E). CD8 immunohistochemistry showed dense CD8$^+$ T cell infiltrates in the periphery of the lesion (Fig. 1F/G), while a mild infiltration of CD8$^+$ T cells was found within the tumor (focally moderate around the necrotic areas; Fig. 1H/I). As a consequence of progressive disease, the planned resection of the gluteal metastasis was not performed.

A similar [^{89}Zr]Zr-Df-IAB22M2C uptake pattern was observed in Patient 7 after four cycles of combined ICT until 6 weeks before the [^{89}Zr]Zr-Df-IAB22M2C PET/MRI. Here, different lymph nodes, which were described as suspicious for metastases in the previous routine [^{18}F]FDG PET/CT performed five weeks earlier (e.g. the hilar lymph node metastasis) showed only a weak [^{89}Zr]Zr-Df-IAB22M2C uptake (Fig. 2A), whereas an axillary lymph node metastasis revealed an intense [^{89}Zr]Zr-Df-IAB22M2C uptake (Fig. 2B). The corresponding [^{18}F]FDG PET/CT which indicated an intense glucose metabolism of both metastases (Fig. 2C/D). Interestingly, a follow up [^{18}F]FDG PET/CT 8 weeks after the [^{89}Zr]Zr-Df-IAB22M2C PET/MRI revealed regression of the CD8 PET/MRI positive axillary lymph node metastasis, while the CD8 PET/MRI negative hilar lymph node metastasis increased in volume and [^{18}F]FDG uptake (Fig. 2E/F).

Patient 3 presented with a brain metastasis which was irradiated nine months before the [^{89}Zr]Zr-Df-IAB22M2C PET/MRI and revealed no tracer uptake above the background (Supplementary Fig. 1A). The histopathological analysis of the brain metastasis six weeks after the PET/MRI revealed white and grey matter interspersed with gemistocytic astrocytes, together with necrotic tissue without viable malignant cells, consistent with post-radiotherapy status (Supplementary Fig. 1B). The CD8 immunohistochemistry showed CD8$^+$ T cells perivascularly nearby the necrotic areas, while only a few CD8$^+$ T cells were identified in the brain parenchyma and necrotic areas (Supplementary Fig. 1C). In the left pararenal gland, where a residual metastasis was located (constant over years), we observed a relatively low [^{89}Zr]Zr-Df-IAB22M2C uptake (SUVmean 4.5).

Multiple lymph nodes (predominantly in the cervical and thoracic region) with an intense [^{89}Zr]Zr-Df-IAB22M2C uptake most likely associated with inflammatory processes were found in 6 out of 8 patients. A metastatic spread in these lymph nodes appeared implausible when considering previous clinical CT or [^{18}F]FDG PET/CT imaging and the clinical history of the patients. These considerably inflammatory lymph nodes with a very high [^{89}Zr]Zr-Df-IAB22M2C uptake were observed in four out of five patients with previous ICT treatment (Fig. 3A). However, two out of three patients without ICT (Patient 4 and Patient 5) showed the identical phenomenon (Fig. 3B).

The comparison of [^{89}Zr]Zr-Df-IAB22M2C and [^{18}F]FDG PET in the NSCLC patient without ICT (Patient 5) revealed multiple mediastinal lymph nodes with moderate [^{89}Zr]Zr-Df-IAB22M2C uptake next to the primary tumor (Fig. 4A-C), which however were not considered to be suspicious in the previous [^{18}F]FDG PET/CT scan (Fig. 4D-F). This, suggests a non-metastatic, inflammatory process as the main cause for the pronounced [^{89}Zr]Zr-Df-IAB22M2C uptake in these lymph nodes.

In our cohort, the intense [^{89}Zr]Zr-Df-IAB22M2C uptake of non-metastatic lymph nodes was not associated with a therapeutic response as we observed identical [^{89}Zr]Zr-Df-IAB22M2C uptake pattern in lymph nodes in both ICT responsive as well as non-responsive metastatic tumor patients (Fig. 3A/B).

Surprisingly, four out of five patients, which underwent ICT before the CD8 PET/MRI exhibited a strongly pronounced [^{89}Zr]Zr-Df-IAB22M2C uptake in the bone marrow (Fig. 5A). Interestingly, we observed in patients without ICT pretreatment a generally lower [^{89}Zr]Zr-Df-IAB22M2C uptake in the bone marrow when compared to the bone marrow of most of the ICT pretreated patients (Fig. 5A; Table 1).

The spleen appeared as the organ with the highest [^{89}Zr]Zr-Df-IAB22M2C uptake in all patients regardless of the tumor entity and the patients' pretreatment. Moreover, the splenic [^{89}Zr]Zr-Df-IAB22M2C uptake displayed a high variability in our patients without any correlation to ICT pretreatment or therapy response (Fig. 5B).

Six out of eight patients exhibited progressive disease in the subsequent weeks and months after the [^{89}Zr]Zr-Df-IAB22M2C PET/MRI. Strikingly, both patients with a long term remission upon ICT (Patient 3 and 4; longer than one year remission) displayed a spleen to liver ratio higher than 8.7 (Fig. 5C) and a relatively high [^{89}Zr]Zr-Df-IAB22M2C uptake in the lymph nodes compared to the other patients (Fig. 3A/B). In contrast, a lower spleen to liver ratio and a lower lymph node uptake was associated with cancer progression in four out of six patients.

Discussion

To date cancer immunotherapies such as ICT are broadly available for multiple tumor entities. However, the diagnostic capabilities to differentiate responders from non-responders are still insufficient and available imaging modalities are limited in predicting therapy response or irAE. [^{18}F]FDG PET/CT is widely used as a very sensitive method for initial staging and monitoring of various cancer types as well as response assessment to therapy [21, 22]. However, this method lacks in specificity, especially with regard to its application to ICT. Reinfeld et al. recently revealed that a large proportion of the glucose metabolism as measured by [^{18}F]FDG PET is not exclusively related to viable tumor cells but also to activated immune cells [23].

Although the exact immunological processes in ICT treated patients remain elusive, CD8$^+$ T cells are critically involved in the ICT-induced anti-tumoral immune response [24]. In recent years several efficient immune cell tracking approaches have been developed but the translatability of many preclinical approaches into clinical application is problematic [25, 26]. The radiolabeled antibody fragment (minibody) [^{89}Zr]Zr-Df-IAB22M2C has been engineered to improve the disadvantages of full antibodies for *in vivo* imaging in particular by reducing the long plasma half-life. To avoid interactions with Fc receptors and the associated immune activation, the Fc region was replaced by a pharmacologically inert domain.

Here, we present first clinical experiences with [^{89}Zr]Zr-Df-IAB22M2C PET/MRI in eight patients under or eligible for ICT. Within our small retrospective patient cohort we detected an elevated CD8 dependent [^{89}Zr]Zr-Df-IAB22M2C uptake in two metastases of two patients. Unfortunately, the two [^{89}Zr]Zr-Df-IAB22M2C accumulating lesions were not eligible for resection. Thus, we were unable to cross validate the elevated [^{89}Zr]Zr-Df-IAB22M2C tracer uptake

by CD8 immunohistochemistry. Nevertheless, two of the metastases without enhanced [^{89}Zr]Zr-Df-IAB22M2C uptake were resected: the pararenal metastasis of Patient 1 and the brain metastasis of Patient 3. CD8 immunohistochemistry of the pararenal metastasis revealed a very faint CD8$^+$ T cell infiltrate in the center of the metastasis, thus well cross-validating the lack of [^{89}Zr]Zr-Df-IAB22M2C uptake. Strikingly, some areas with a dense infiltration of CD8$^+$ T cells were found at the margins of the metastasis. The immunohistochemistry staining for CD8 in Fig. 1F is demonstrating that the dense infiltration of CD8$^+$ T cells are located in a very thin layer at the margin of the lesion. As this layer has only a thickness in the micrometer scale and only few CD8$^+$ T cells were located in the tumor center, partial volume effect could explain why this infiltration of CD8$^+$ T cells at the margin was not reflected by the [^{89}Zr]Zr-Df-IAB22M2C PET images.

In the case of the brain metastasis of Patient 3 the breakdown of the blood brain barrier in melanoma metastasis should enable a sufficient delivery of the tracer into the malignant tissue. Since there are only very few CD8$^+$ T cells located in this metastasis according to immunohistochemistry (Supplementary Fig. 1) no relevant uptake was observed in the [^{89}Zr]Zr-Df-IAB22M2C PET.

In recent years, it became evident that the amount and the localization of T cell infiltration in the tumor is a major predictor of the patient outcome [27–29]. The distinction of a) immunological „hot“ tumors with dense immune infiltrates, b) immune „deserts“ without relevant immune infiltrate as well as c) immune excluded tumors with an immune infiltrate at the tumor margins has been proposed by different authors [30, 31]. The CD8 immunohistochemistry of the pararenal metastasis of patient 1 correlated very well with the non-invasive CD8 PET/MR imaging and would classify the lesion into the so called immune „excluded“ phenotype. Nevertheless, larger scale prospective trials with histological cross-validation are needed to validate whether [^{89}Zr]Zr-Df-IAB22M2C PET is applicable to distinguish immunological „hot“ tumors with a dense immune infiltrate from immune excluded or immune deserted tumors.

In addition, it has to be considered that the presence of CD8$^+$ T cells does not guarantee the functionality of the CD8$^+$ T cells. Consequently, additional characterization of the tumor microenvironment like metabolic parameters (glucose metabolism, lactate production), or acidity (pH) etc. might be necessary to further evaluate the effectivity of the T cell infiltrate in regard of an efficient anti tumoral immune response.

Upon ICT the primary and secondary lymphatic organs are considered to be highly involved in the elicited systemic immune response in cancer patients.

Recently, our group performed preclinical translational as well as prospective clinical studies with [^{18}F]FDG PET for the assessment of metabolic changes in primary and secondary lymphoid organs before and upon ICT in order to visualize and quantify the systemic response [21, 32]. These studies showed that an elevated splenic glucose metabolism was related to responsiveness to ICT [32] and may serve as an early treatment response marker [21]. In addition, we observed that the glucose metabolism in the bone marrow, a primary lymphatic organ, was increased in patients responsive to ICT. Interestingly, an elevated glucose metabolism in the bone marrow even before start of ICT was applicable to predict treatment response [21, 32]. Nevertheless, it has to be considered that the increased, but probably relatively unspecific glucose metabolism in the primary and secondary lymphatic organs, might be a feature which can be found also in a variety of both physiological and pathological conditions.

In our patient cohort a high interpatient variability of the [^{89}Zr]Zr-Df-IAB22M2C uptake within the primary and secondary lymphoid organs was observed. Non-malignant lymph nodes with a high [^{89}Zr]Zr-Df-IAB22M2C uptake were found in the majority of the patients especially in the cervical and thoracic region. Interestingly, presence or absence of ICT treatment didn't impact the elevated [^{89}Zr]Zr-Df-IAB22M2C uptake in these lymph nodes.

Generally CD8$^+$ T cells are critically involved in adaptive immune responses including the elimination of malignant cells but also e.g. in the removal of virus infected cells [17]. Therefore, obviously a lot of physiologic and pathologic processes within the primary and secondary lymphatic organs might influence the [^{89}Zr]Zr-Df-IAB22M2C biodistribution. Thus, patient specific physiological (aged immune system etc.) and pathological processes (viral infections etc.) might interfere with the holistic [^{89}Zr]Zr-Df-IAB22M2C PET signature.

Interestingly, 4 out of 6 patients with tumor progression upon ICT tended towards a lower spleen to liver ratio in comparison to the two ICT responsive patients which were in remission. These findings are in line with preclinical data, where ICT-induced glucose metabolism of the spleen was associated to an elevated number of neutrophils and a reduced number of infiltrating T cells [32]. In accordance to this, our prospective study mentioned above revealed an elevated [^{18}F]FDG uptake in the spleen of most ICT responsive patients, while non-responsive patients did not exhibit any significant differences. Moreover, multiple reasons for dysfunctional CD8$^+$ T cells within the tumor microenvironment have been discovered which are major hurdles for ICT efficacy [13].

Because [^{89}Zr]Zr-Df-IAB22M2C PET alone might be not applicable to evaluate the functionality of CD8$^+$ T cells. Thus, dual tracer approaches might be required for identification of efficient CD8$^+$ T cell functioning and potentially enable the detection of therapy response. As second tracer beside [^{89}Zr]Zr-Df-IAB22M2C newly developed tracers like [^{18}F]-arabinosyl guanine [33] and the granzyme B targeting tracer [^{68}Ga]-NOTA-GZP [34] might provide additional information on T cell functionality. However, also conventional [^{18}F]FDG could potentially give evidence towards T cell activation as we were able to demonstrate previously that the distribution of [^{18}F]FDG in primary and secondary lymphoid organs is accompanied with successful cancer immune responses [32].

Subsequent prospective clinical studies are needed to explore how reliable these patterns are and whether they allow a treatment stratification in order to improve the therapeutic outcome of patients with metastasized cancer.

Conclusion

Our first clinical experiences revealed the feasibility of [^{89}Zr]Zr-Df-IAB22M2C PET/MRI to assess potential immune-related changes in the CD8 expression within metastases and the primary and secondary lymphatic organs. The results suggest that the distribution of $CD8^+$ T cells in the lymphatic organs as assessed by [^{89}Zr]Zr-Df-IAB22M2C PET might be associated with the systemic immune response induced by ICT. Further prospective clinical trials are needed to gain deeper insights into the relationship of the detected $CD8^+$ T cell distribution and response to ICT.

Declarations

Acknowledgments

This work was supported by the Deutsche Forschungsgemeinschaft (DFG, German Research Foundation, Germany´s Excellence Strategy-EXC2180-390900677) and the Werner Siemens-Foundation.

Funding

This work was supported by the Deutsche Forschungsgemeinschaft (DFG, German Research Foundation, Germany´s Excellence Strategy-EXC2180-390900677) and the Werner Siemens-Foundation.

Competing Interests

R.K. and I.W. are employees from ImaginAB. ClF is an advisor of ImaginAB. The other authors report no conflict of interest.

Author Contributions

JS and ClF analyzed the PET/MRI data and the interpretated together with DSo, PK, IW, RK, FS, AF, TE, LZ, MR, BP, LF and MK. DSe, WE, GK and GR produced the radiotracer. IGM and LQM performed and analyzed the histology and immunohistochemistry. JS, MK and ClF wrote the manuscript, and all authors read and approved the final manuscript.

Ethics approval

The PET/MRI scans were performed following the stipulations of the German medicinal products act (“Arzneimittelgesetz”; AMG) §13(2b). The retrospective analysis was approved by the approved by the institutional review board (permit 534/2021BO2).

Consent to participate

Informed consent was obtained from all individual participants included in the study.

References

1. Terheyden P, Krackhardt A, Eigentler T. The Systemic Treatment of Melanoma. Dtsch Arztebl Int. 2019;116:497-504. doi:10.3238/arztebl.2019.0497.
2. Rotte A. Combination of CTLA-4 and PD-1 blockers for treatment of cancer. J Exp Clin Cancer Res. 2019;38:255. doi:10.1186/s13046-019-1259-z.
3. Garbe C, Amaral T, Peris K, Hauschild A, Arenberger P, Bastholt L, et al. European consensus-based interdisciplinary guideline for melanoma. Part 1: Diagnostics - Update 2019. Eur J Cancer. 2020;126:141-58. doi:10.1016/j.ejca.2019.11.014.
4. Schreiber RD, Old LJ, Smyth MJ. Cancer immunoediting: integrating immunity's roles in cancer suppression and promotion. Science. 2011;331:1565-70. doi:10.1126/science.1203486.
5. Wieder T, Eigentler T, Brenner E, Rocken M. Immune checkpoint blockade therapy. J Allergy Clin Immunol. 2018;142:1403-14. doi:10.1016/j.jaci.2018.02.042.
6. Postow MA, Sidlow R, Hellmann MD. Immune-Related Adverse Events Associated with Immune Checkpoint Blockade. N Engl J Med. 2018;378:158-68. doi:10.1056/NEJMra1703481.
7. Martins F, Sofiya L, Sykiotis GP, Lamine F, Maillard M, Fraga M, et al. Adverse effects of immune-checkpoint inhibitors: epidemiology, management and surveillance. Nat Rev Clin Oncol. 2019;16:563-80. doi:10.1038/s41571-019-0218-0.
8. Wei SC, Anang NAS, Sharma R, Andrews MC, Reuben A, Levine JH, et al. Combination anti-CTLA-4 plus anti-PD-1 checkpoint blockade utilizes cellular mechanisms partially distinct from monotherapies. Proc Natl Acad Sci U S A. 2019;116:22699-709. doi:10.1073/pnas.1821218116.
9. Hegde PS, Chen DS. Top 10 Challenges in Cancer Immunotherapy. Immunity. 2020;52:17-35. doi:10.1016/j.immuni.2019.12.011.
10. Spitzer MH, Carmi Y, Reticker-Flynn NE, Kwek SS, Madhireddy D, Martins MM, et al. Systemic Immunity Is Required for Effective Cancer Immunotherapy. Cell. 2017;168:487-502 e15. doi:10.1016/j.cell.2016.12.022.
11. Allen BM, Hiam KJ, Burnett CE, Venida A, DeBarge R, Tenvooren I, et al. Systemic dysfunction and plasticity of the immune macroenvironment in cancer models. Nat Med. 2020;26:1125-34. doi:10.1038/s41591-020-0892-6.
12. Tumeh PC, Harview CL, Yearley JH, Shintaku IP, Taylor EJ, Robert L, et al. PD-1 blockade induces responses by inhibiting adaptive immune resistance. Nature. 2014;515:568-71. doi:10.1038/nature13954.

13. van der Leun AM, Thommen DS, Schumacher TN. CD8(+) T cell states in human cancer: insights from single-cell analysis. Nat Rev Cancer. 2020;20:218-32. doi:10.1038/s41568-019-0235-4.
14. Devine L, Kavathas PB. Molecular analysis of protein interactions mediating the function of the cell surface protein CD8. Immunol Res. 1999;19:201-10. doi:10.1007/BF02786488.
15. Moebius U, Kober G, Griscelli AL, Hercend T, Meuer SC. Expression of different CD8 isoforms on distinct human lymphocyte subpopulations. Eur J Immunol. 1991;21:1793-800. doi:10.1002/eji.1830210803.
16. Sathaliyawala T, Kubota M, Yudanin N, Turner D, Camp P, Thome JJ, et al. Distribution and compartmentalization of human circulating and tissue-resident memory T cell subsets. Immunity. 2013;38:187-97. doi:10.1016/j.immuni.2012.09.020.
17. Zhang N, Bevan MJ. CD8(+) T cells: foot soldiers of the immune system. Immunity. 2011;35:161-8. doi:10.1016/j.immuni.2011.07.010.
18. Pandit-Taskar N, Postow MA, Hellmann MD, Harding JJ, Barker CA, O'Donoghue JA, et al. First-in-Humans Imaging with (89)Zr-Df-IAB22M2C Anti-CD8 Minibody in Patients with Solid Malignancies: Preliminary Pharmacokinetics, Biodistribution, and Lesion Targeting. J Nucl Med. 2020;61:512-9. doi:10.2967/jnumed.119.229781.
19. Farwell MD, Gamache RF, Babazada H, Hellmann MD, Harding JJ, Korn R, et al. CD8-targeted PET Imaging of Tumor Infiltrating T cells in Patients with Cancer: A Phase I First-in-Human Study of (89)Zr-Df-IAB22M2C, a Radiolabeled anti-CD8 Minibody. J Nucl Med. 2021. doi:10.2967/jnumed.121.262485.
20. Farwell MD, Gamache RF, Babazada H, Hellmann MD, Harding JJ, Korn R, et al. CD8-targeted PET Imaging of Tumor Infiltrating T cells in Patients with Cancer: A Phase I First-in-Human Study of (89)Zr-Df-IAB22M2C, a Radiolabeled anti-CD8 Minibody. J Nucl Med. 2021. doi:10.2967/jnumed.121.262485.
21. Seith F, Forschner A, Weide B, Guckel B, Schwartz M, Schwenck J, et al. Is there a link between very early changes of primary and secondary lymphoid organs in (18)F-FDG-PET/MRI and treatment response to checkpoint inhibitor therapy? J Immunother Cancer. 2020;8. doi:10.1136/jitc-2020-000656.
22. Bisschop C, de Heer EC, Brouwers AH, Hospers GAP, Jalving M. Rational use of (18)F-FDG PET/CT in patients with advanced cutaneous melanoma: A systematic review. Crit Rev Oncol Hematol. 2020;153:103044. doi:10.1016/j.critrevonc.2020.103044.
23. Reinfeld BI, Madden MZ, Wolf MM, Chytil A, Bader JE, Patterson AR, et al. Cell-programmed nutrient partitioning in the tumour microenvironment. Nature. 2021;593:282-8. doi:10.1038/s41586-021-03442-1.
24. Kurtulus S, Madi A, Escobar G, Klapholz M, Nyman J, Christian E, et al. Checkpoint Blockade Immunotherapy Induces Dynamic Changes in PD-1(-)CD8(+) Tumor-Infiltrating T Cells. Immunity. 2019;50:181-94 e6. doi:10.1016/j.immuni.2018.11.014.
25. Thunemann M, Schorg BF, Feil S, Lin Y, Voelkl J, Golla M, et al. Cre/lox-assisted non-invasive in vivo tracking of specific cell populations by positron emission tomography. Nat Commun. 2017;8:444. doi:10.1038/s41467-017-00482-y.
26. Griessinger CM, Maurer A, Kesenheimer C, Kehlbach R, Reischl G, Ehrlichmann W, et al. 64Cu antibody-targeting of the T-cell receptor and subsequent internalization enables in vivo tracking of lymphocytes by PET. Proc Natl Acad Sci U S A. 2015;112:1161-6. doi:10.1073/pnas.1418391112.
27. Galon J, Costes A, Sanchez-Cabo F, Kirilovsky A, Mlecnik B, Lagorce-Pages C, et al. Type, density, and location of immune cells within human colorectal tumors predict clinical outcome. Science. 2006;313:1960-4. doi:10.1126/science.1129139.
28. Pages F, Mlecnik B, Marliot F, Bindea G, Ou FS, Bifulco C, et al. International validation of the consensus Immunoscore for the classification of colon cancer: a prognostic and accuracy study. Lancet. 2018;391:2128-39. doi:10.1016/S0140-6736(18)30789-X.
29. Camus M, Tosolini M, Mlecnik B, Pages F, Kirilovsky A, Berger A, et al. Coordination of intratumoral immune reaction and human colorectal cancer recurrence. Cancer Res. 2009;69:2685-93. doi:10.1158/0008-5472.CAN-08-2654.
30. Hegde PS, Karanikas V, Evers S. The Where, the When, and the How of Immune Monitoring for Cancer Immunotherapies in the Era of Checkpoint Inhibition. Clin Cancer Res. 2016;22:1865-74. doi:10.1158/1078-0432.CCR-15-1507.
31. Chen DS, Mellman I. Elements of cancer immunity and the cancer-immune set point. Nature. 2017;541:321-30. doi:10.1038/nature21349.
32. Schwenck J, Schorg B, Fiz F, Sonanini D, Forschner A, Eigentler T, et al. Cancer immunotherapy is accompanied by distinct metabolic patterns in primary and secondary lymphoid organs observed by non-invasive in vivo (18)F-FDG-PET. Theranostics. 2020;10:925-37. doi:10.7150/thno.35989.
33. Levi J, Lam T, Goth SR, Yaghoubi S, Bates J, Ren G, et al. Imaging of Activated T Cells as an Early Predictor of Immune Response to Anti-PD-1 Therapy. Cancer Res. 2019;79:3455-65. doi:10.1158/0008-5472.CAN-19-0267.
34. Larimer BM, Wehrenberg-Klee E, Dubois F, Mehta A, Kalomeris T, Flaherty K, et al. Granzyme B PET Imaging as a Predictive Biomarker of Immunotherapy Response. Cancer Res. 2017;77:2318-27. doi:10.1158/0008-5472.CAN-16-3346.

Figures

Figure 1

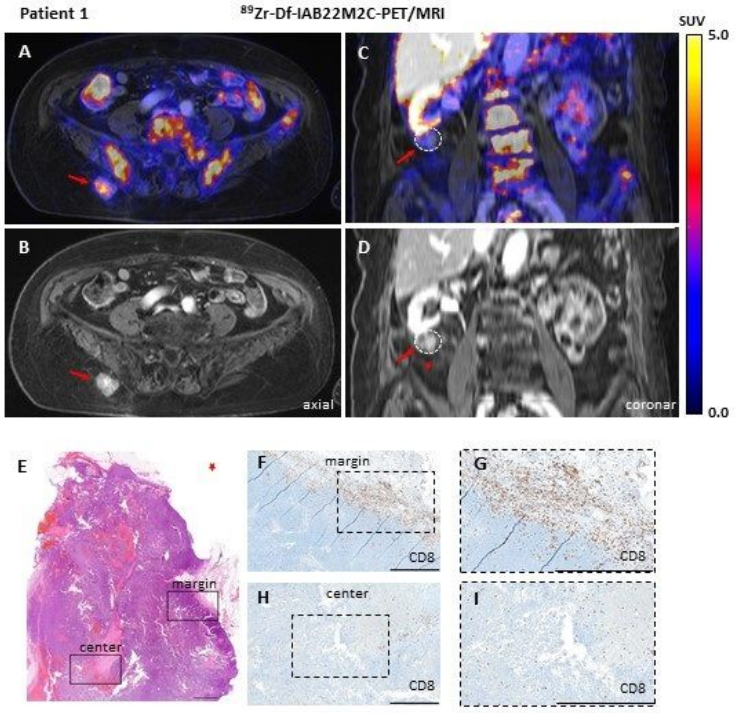

Figure 1

A/B: Axial fused [^{89}Zr]Zr-Df-IAB22M2C PET/MRI and MRI of a metastasis with intense tracer uptake in the right gluteal subcutaneous tissue of Patient 1 after three cycles of ipilimumab until 6 weeks before the scan. **C/D:** Coronal fused ^{89}Zr]Zr-Df-IAB22M2C PET/MRI and MRI of a pararenal metastasis of Patient 1 without relevant [tracer uptake after ipilimumab treatment. **E-I:** The pararenal metastasis of Patient 1 (red star) was resected. **E:** Histopathological analysis revealed a monotonous cell proliferation in the metastasis. The immunohistochemistry revealed some areas with dense infiltrates of CD8$^+$ T cells in the margin of the lesion **(H)**; magnification **(I)**, while only mild infiltration of CD8$^+$ T cells in the center of the metastasis (focally moderate around the necrotic areas) was observed **(F)**; magnification **(G).** Scale: 1mm for both H&E and CD8 immunohistochemistry images.

Figure 2

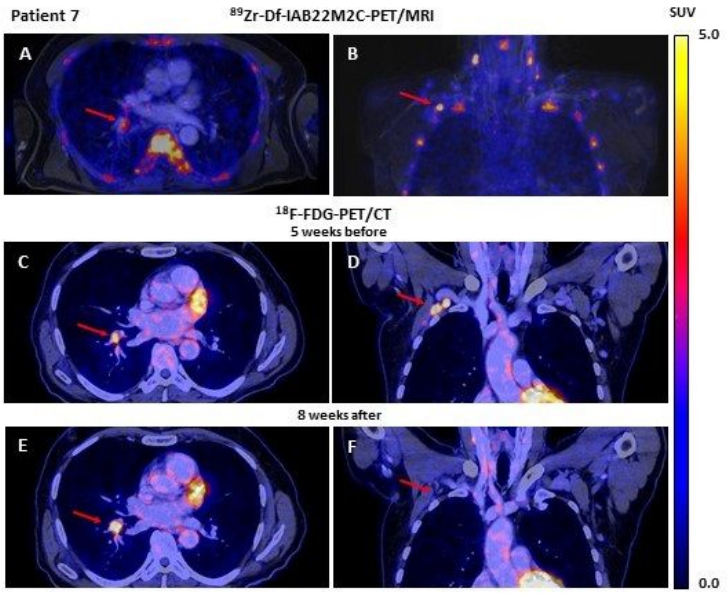

Figure 2

A/B: Fused [^{89}Zr]Zr-Df-IAB22M2C PET/MRI of Patient 7 after 4 cycles of combined ICT using ipilimumab and nivolumab until 6 weeks before the scan indicated only a faint tracer uptake in a hilar lymph node metastasis **(A)**, whereas an intense tracer uptake was found in an axillary lymph node metastasis (B). **C/D:** Fused [^{18}F]FDG PET/CT images of Patient 7 five weeks before [^{89}Zr]Zr-Df-IAB22M2C PET/MRI, indicated an intense glucose uptake of both the axillary and the hilar lymph node metastasis, which thus were considered to be viable tumor tissue. **E/F:** Eight weeks after the [^{89}Zr]Zr-Df-IAB22M2C PET/MRI the follow up [^{18}F]FDG PET/CT of Patient 7 revealed a decrease of the axillary lymph node metastasis under ICT, while the hilar lymph node metastasis increased in size and [^{18}F]FDG uptake under ICT-monotherapy with Nivolumab.

Figure 3

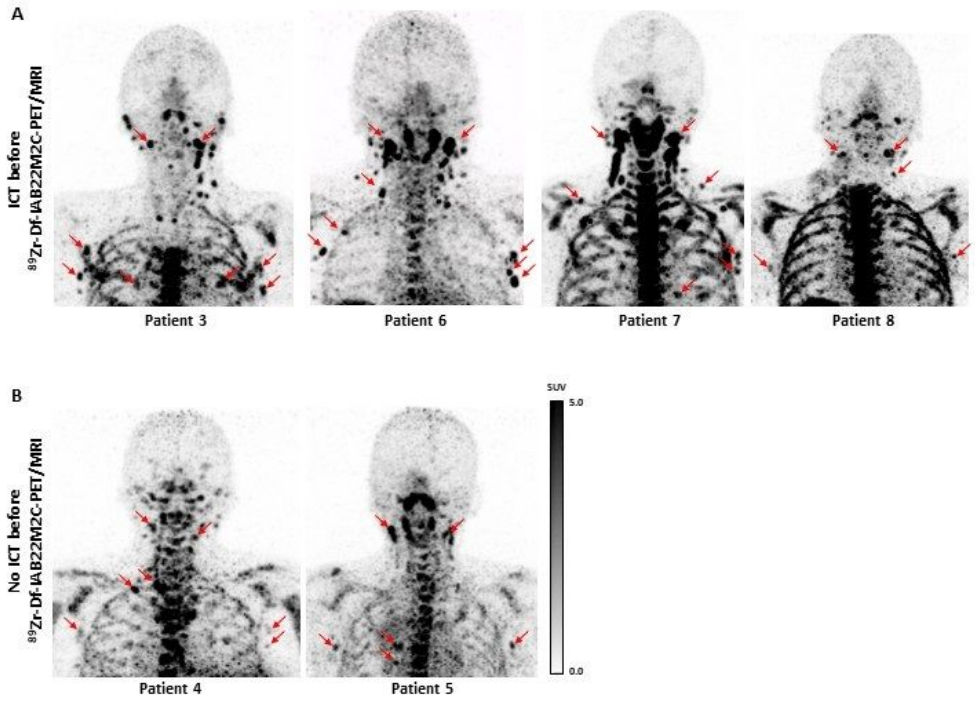

Figure 3

A: In Patient 3, 6, 7 and 8 with ICT pretreatment multiple lymph nodes with an intense [^{89}Zr]Zr-Df-IAB22M2C uptake located predominantly in the cervical and thoracic region were identified. Considering the previous routine imaging and the clinical history of the patients, these lymph nodes appeared rather associated with inflammatory processes than metastases. **B:** In Patient 4 and 5 without ICT pretreatment an intense [^{89}Zr]Zr-Df-IAB22M2C uptake in the lymph nodes was evident. These lymph nodes have been considered as non-malignant according to the previous routine imaging and the clinical history.

Figure 4

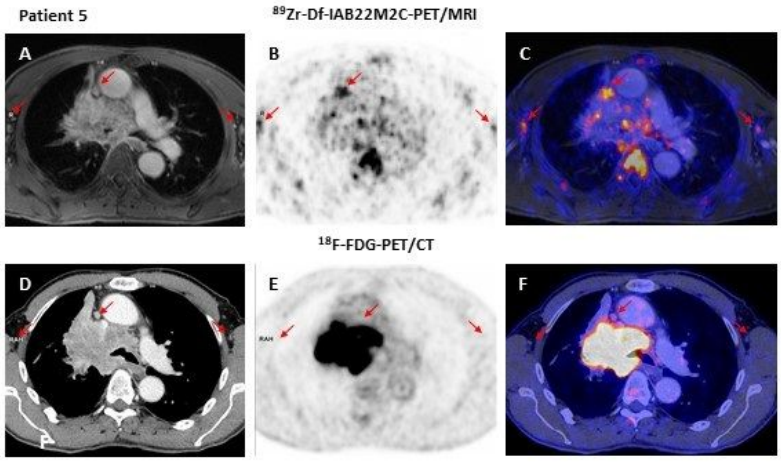

Figure 4

A-C: Patient 5 presented with a moderate [^{89}Zr]Zr-Df-IAB22M2C uptake in several mediastinal lymph nodes next to the primary tumor independent of any previous cancer treatment. **D-F:** In the previous [^{18}F]FDG PET/CT scan the mediastinal lymph nodes of Patient 5 have not been considered suspicious for metastasis.

Figure 5

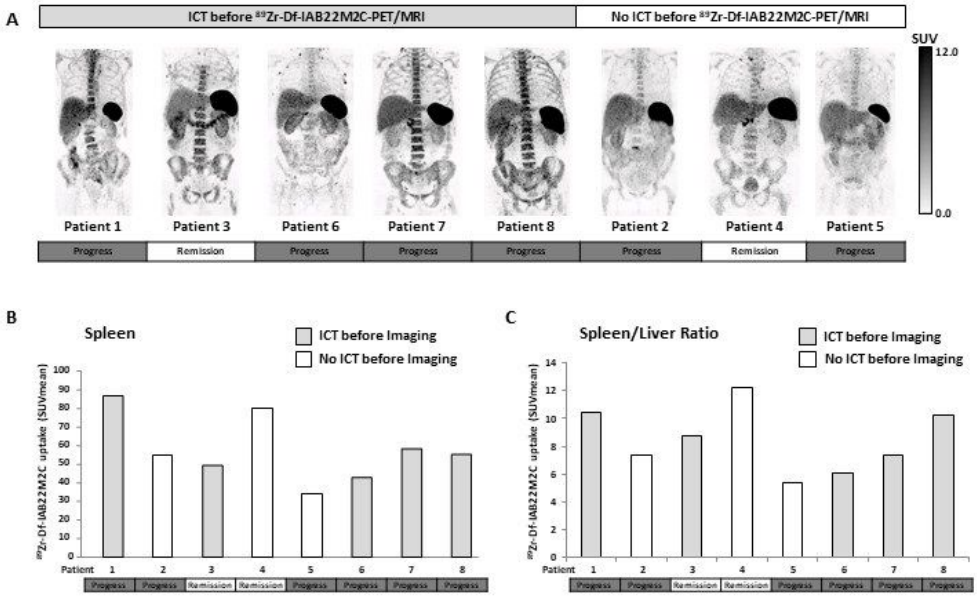

Figure 5

A: A high [^{89}Zr]Zr-Df-IAB22M2C uptake in the bone marrow was observed in the majority of the patients with ICT pretreatment, whereas patients without ICT pretreatment exhibited a relatively low [^{89}Zr]Zr-Df-IAB22M2C uptake in the bone marrow. **B:** A high variability of splenic [^{89}Zr]Zr-Df-IAB22M2C uptake was determined in our patients cohort independent from ICT pretreatment or therapy response.

C: The ratio of spleen to liver [^{89}Zr]Zr-Df-IAB22M2C uptake was not directly correlated with previous ICT. Nevertheless, both patients with a long term remission (>one year remission under ICT; Patient 3 and 4) displayed a considerable high spleen to liver ratio.

Supplementary Files

This is a list of supplementary files associated with this preprint. Click to download.

- FigS1.jpg